Construction of RNA–Quantum Dot Chimera for Nanoscale Resistive Biomemory Application

Taek Lee,[†] Ajay Kumar Yagati,[‡] Fengmei Pi,[†] Ashwani Sharma,[†] Jeong-Woo Choi,[*,§] and Peixuan Guo[*,†]

[†]Nanobiotechnology Center, Markey Cancer Center, and Department of Pharmaceutical Sciences, University of Kentucky, Lexington, Kentucky 40536, United States, [‡]Department of Biomedical Engineering, Gachon University, 191 Hambakmoero, Yeonsu-gu, Incheon 406-799, Republic of Korea, and [§]Department of Chemical and Biomolecular Engineering, Sogang University, 35 Baekbeom-ro (Sinsu-dong), Mapo-gu, Seoul 121-742, Republic of Korea

ABSTRACT RNA nanotechnology offers advantages to construct thermally and chemically stable nanoparticles with well-defined shape and structure. Here we report the development of an RNA–QD (quantum dot) chimera for resistive biomolecular memory application. Each QD holds two copies of the pRNA three-way junction (pRNA-3WJ) of the bacteriophage phi29 DNA packaging motor. The fixed quantity of two RNAs per QD was achieved by immobilizing the pRNA-3WJ with a Sephadex aptamer for resin binding. Two thiolated pRNA-3WJ serve as two feet of the chimera that stand on the gold plate. The RNA nanostructure served as both an insulator and a mediator to provide defined distance between the QD and gold. Immobilization of the chimera nanoparticle was confirmed with scanning tunneling microscopy. As revealed by scanning tunneling spectroscopy, the conjugated pRNA-3WJ–QD chimera exhibited an excellent electrical bistability signal for biomolecular memory function, demonstrating great potential for the development of resistive biomolecular memory and a nano-bio-inspired electronic device for information processing and computing.

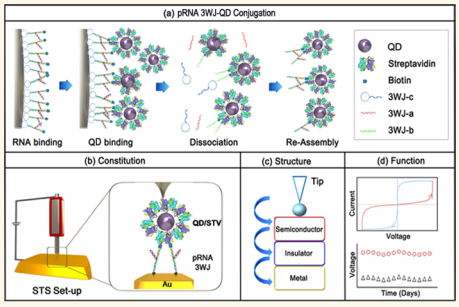

KEYWORDS: RNA nanotechnology · pRNA–quantum dot chimera · biomolecular electronics · nanoscale resistive biomolecular memory · phi29 DNA packaging motor

In 1965, Gordon Moore anticipated that the number of transistors and memory devices per unit area on an integrated circuit would double every year due to the expansion of information.[1] Subsequently, advances in memory devices, transistors, and information processors have moved to microsized dimensions.[1,2] The random access memory (RAM) devices are essential for microsized computing machines. RAMs are fast, but they are volatile and energy-consuming. Si-Flash memory devices represent prominent nonvolatile data memory[3] due to high density and low production costs but suffer from low endurance and low write speed and require high voltages for write operations. Thus, the semiconductor industry faces many challenges such as integration limitation, heat induction, and energy efficiency. To overcome current limitations, some pioneers of the field proposed molecular electronics,[4,5] which showed potential for molecular-level size control and fabrication. Molecular memory devices such as virus-based particles[6] and protein-based or inorganic molecule-based devices[7−10] have shown promise. However, the addressability of the systems to fabricate molecular memory devices with controllable block assembly utilizing a bottom-up approach is still limited. Thus, well-defined and easy to assemble nanostructures are needed. Bottom-up assembly using proteins or other macromolecules is more challenging due to the complexity in structure, folding, and molecular interaction during assembly. Development of nanoscale resistive biomemory[11] based on RNA nanotechnology[12] could be an advantageous alternative, especially due to the recently reported addressable bottom-up self-assembly property of the three-way junction of bacteriophage phi29 motor pRNA.[13]

The concept of RNA nanotechnology was first proven in 1998[14] using packaging RNA (pRNA)[15] derived from the bacteriophage phi29 DNA packaging motor. RNA dimers, trimers, and hexamers were assembled

* Address correspondence to peixuan.guo@uky.edu, jwchoi@sogang.ac.kr.

Received for review May 31, 2015 and accepted July 2, 2015.

Published online July 02, 2015
10.1021/acsnano.5b03269

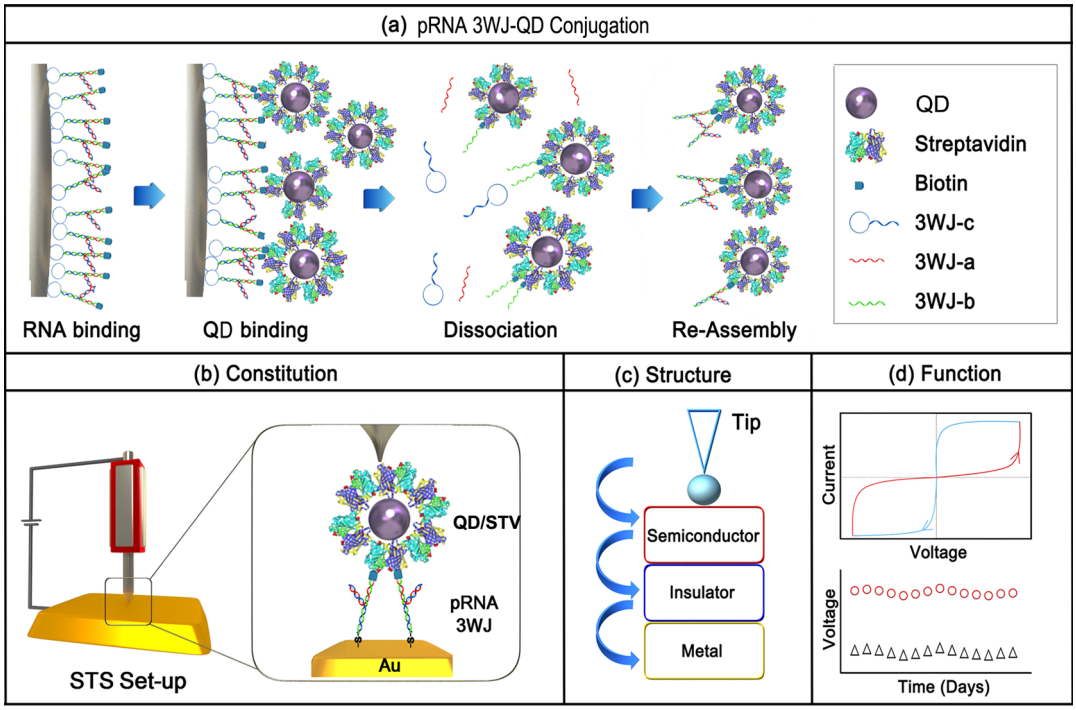

Figure 1. Schematic diagram of the experimental design. (a) Site-specific conjugation method for the QD/STVQD/STV/Bio-3WJ chimera nanoparticle, (b) constitution, (c) expected structure, and (d) function.

from re-engineered RNA fragments *via* a bottom-up assembly,[16,17] one of the two nanotechnology approaches besides the top-down approach. The pRNA molecule contains two domains, a helical DNA translocation domain and an intermolecular interaction domain.[12,13,18] These two domains are connected by a three-way junction (3WJ) motif, which has been found recently to be a thermodynamically stable nanostructure motif.[13,19−21] The 3WJ remains intact even when diluted to picomolar concentration and remains stable at boiling temperatures[22] in the presence of a strong denaturing reagent.[13] The thermodynamically stable properties make the pRNA-3WJ motif an ideal building block for constructing various RNA nanoparticles for diverse applications in nanomedicine and nanotechnology.[23] A large number of other highly ordered RNA structures have been reported and shown to perform diverse biological functions.[24−32]

Here we report the use of exceptionally stable pRNA-3WJ to design and construct a new bioinorganic chimera material that displays a bistable resistive switching biomolecular memory property. The pRNA-3WJ was specifically conjugated to the streptavidin-coated quantum dots (QD/STV). The QD/STV/Bio-3WJ-SH (biotin-3WJ-thio) complex contained one QD as the head and two thiol-modified 3WJ as feet (Figure 1a) to stand on the gold plate *via* covalent binding of the SH group (Figure 1b).[33,34] The pRNA-3WJ served as an insulator to prevent the QD from direct contact with the gold (Au) substrate (Figure 1c). This unique structure of the RNA−QD conjugate shows a resistive switching property, as confirmed by scanning tunneling microscopy (STM) and scanning tunneling spectroscopy (STS) in air (Figure 1d).[12,35,36]

RESULTS AND DISCUSSION

Experimental Design. In this study, the QD was used as a semiconducting material to charge and release the electrons. Au was used as a substrate to measure the electric signal. The resistive switching memory utilized the QD, pRNA-3WJ, and Au to study the memory function. QD and Au substrates were separated by pRNA-3WJ, which served both as a connector to the bridge and as a partition to prevent the contact between QD and Au substrates while keeping them at an appropriate distance. The pRNA-3WJ served as an insulator between the QD and Au block (Figure 1c). The pRNA-3WJ and QD were conjugated with a specific binding ratio, with two RNA molecules attached to one QD, thus serving as feet standing on the Au block. The STM experiment was conducted to detect the pRNA-3WJ/QD conjugate on the surface, and the tip was positioned onto the pRNA-3WJ/QD conjugate. The electric potential was applied to the pRNA-3WJ/QD conjugate by utilizing the STS setup, thereby monitoring the resistive switching memory function.

Construction of the RNA−QD Chimera Containing a QD as the Head and the pRNA-3WJ Motif as the Feet To Stand on the Gold Substrate. Five steps were carried out to conjugate QDs with pRNA-3WJ: (1) assemble the 3WJ nanoparticles that contain two functional modules: a biotin and a

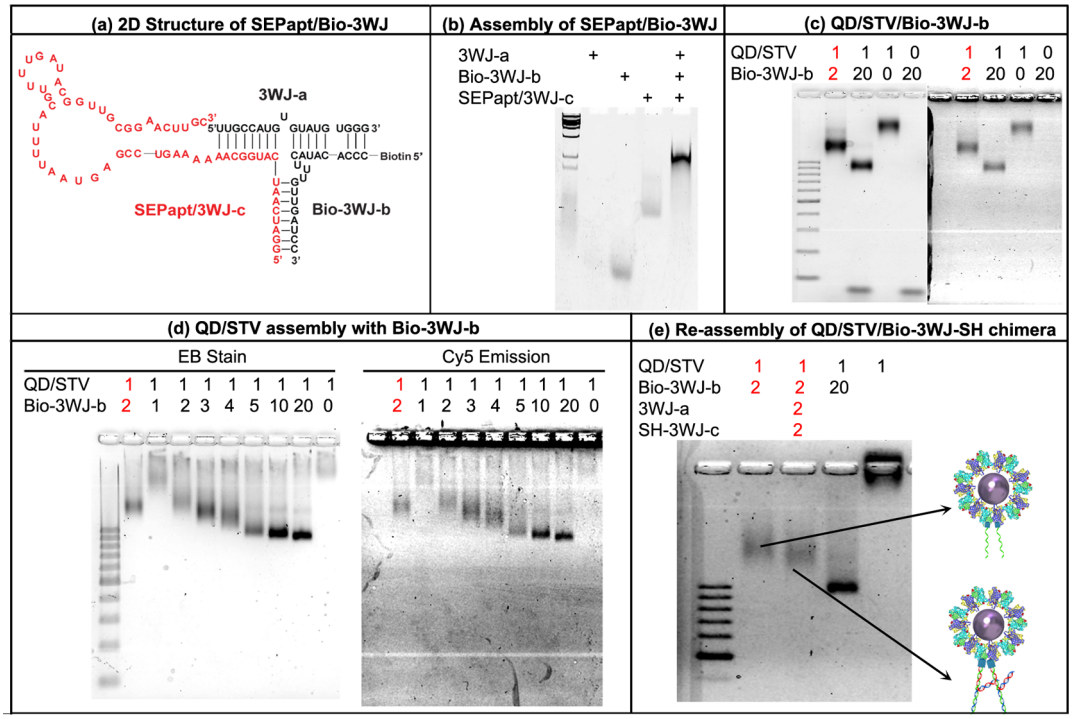

Figure 2. Assay for the assembly of the pRNA-3WJ/QD chimera. (a) Two-dimensional structure of the biotinylated pRNA-3WJ containing an aptamer that can bind Sephadex G100. (b) Native polyacrylamide gel with ethidium bromide staining showing the assembly of the RNA structure in (a). Lane 1 is the DNA ladder. (c) Native agarose (2% TBE) gel image with ethidium bromide staining (left panel) and Cy5 fluorescence emission (right panel) showing the purified QD/STV/Bio-3WJ-b. Lane 1 is a 100 base pair DNA ladder. (d) Native agarose gel imaged with ethidium bromide staining (left panel) and Cy5 fluorescence emission (right panel) to titrate the copy number of Bio-3WJ-b binding to each QD/STV complex using a Sephadex G100 immobilization method. (e) Native agarose gel with ethidium bromide staining shows the reassembled QD/STV/Bio-3WJ-SH chimera after reconjugation. Lanes labeled in red letters show a purified complex, and lanes labeled in black letters show the physical mixture.

Sephadex binding RNA aptamer (SEPapt) (Figure 2a,b); (2) immobilize this SEPapt/Bio-3WJ RNA nanoparticle onto Sephadex resin; (3) incorporate the QD/STV to the Bio-3WJ immobilized on Sephadex resin; 4) dissociate, by urea/EDTA, and purify the QD/STV/Bio-3WJ-b (Figure 2c); (5) reassemble the QD/STV/Bio-3WJ-SH chimera (Figure 2e).

The Sephadex aptamer and biotin did not hamper the formation of the 3WJ. The SEPapt/Bio-3WJ was immobilized onto the Sephadex surface through aptamer recognition. A similar method using an RNA aptamer for RNA nanoparticle affinity purification has been reported.[37,38] QD/STV was conjugated to SEPapt/Bio-3WJ by incubation, and the complex of QD/STV/Bio-3WJ-b was finally eluted from the Sephadex column by adding denaturing reagent to disturb the folding of the Sephadex aptamer and the association of three strands among the 3WJ. The agarose gel in Figure 2c (lane 2) shows the eluted QD/STV/Bio-3WJ-b. In comparison to physical mixture of QD/STV and Bio-3WJ-b (lane 3), the purified QD/STV/Bio-3WJ-b showed a clear single band and slower migration (lane 2). The binding ratios between QD/STV and Bio-3WJ-b were titrated (Figure 2d)[42] and found to be 1:2. Presumably, this ratio originated from the steric hindrance between Bio-3WJ on the Sephadex resin and QD/STV. Once the Bio-3WJ-b bound to the Sephadex resin surface, the accessibility of Bio-3WJ-b to QD/STV was confined. This was due to the spatial configuration of streptavidin that has four biotin binding sites distributed as two pairs that face two directions. Only two biotin binding sites are accessible to Bio-3WJ-b when it is immobilized on Sephadex G100 because the other two sites are not accessible to Bio3WJ-b, and the spherical nature of the QD makes the other sites too far away to reach the 3WJ-b. In comparison to the QD/STV and Bio-3WJ-b physical mixture, the Sephadex aptamer-based conjugation method provides the site-specific and stoichiometry-defined conjugation. Furthermore, the reassembly of QD/STV/Bio-3WJ-SH formation was confirmed by 2% native TBM agarose gel (Figure 2e). Lane 3 shows the reassembled QD/STV/Bio-3WJ-SH, and lane 2 shows the QD/STV/Bio-3WJ-b. The STM images, height analysis, and surface roughness analysis of the conjugates indicated that the QD/STV/Bio-3WJ-SH chimera was well immobilized onto the Au substrate (Supporting Information Figure S1).

Electrical Properties of QD/STV/Bio-3WJ Hybrid Nanoparticle. To confirm the resistive memory property of the pRNA-3WJ/QD chimera at the nanoscale, the QD/STV/Bio-3WJ-SH chimera was immobilized onto a Au substrate at a dilute concentration. The electrical properties of

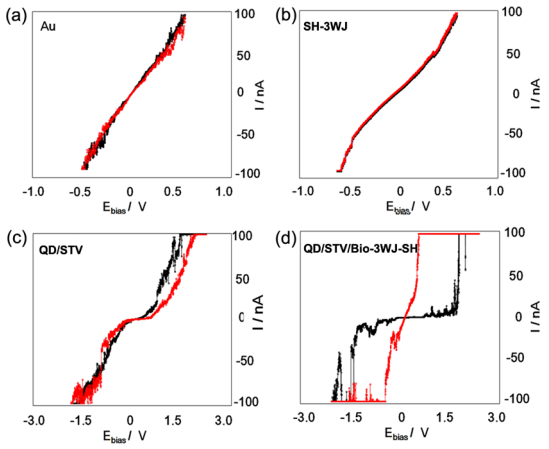

Figure 3. *I*–*V* plot of the QD/STV/Bio-3WJ-SH chimera on the (a) Au surface, (b) thiol-modified pRNA-3WJ on the Au surface, (c) QD/STV adsorbed on the Au surface, and (d) re-assembled QD/STV/Bio-3WJ-SH chimera on the Au surface.

the QD/STV/Bio-3WJ-SH chimera were examined by STS. To compare the electrical property of individual molecules, the thiol-modified pRNA-3WJ and QD/STV were adsorbed onto the Au substrate. *I*–*V* curves of each molecule were measured at room temperature by positioning the conductive tip on top of the sample. Figure 3a–d shows electrical *I*–*V* properties of Au, thiol-modified pRNA-3WJ, QD/STV, and the QD/STV/Bio-3WJ-SH chimera. In the case of bare Au, only a linear *I*–*V* characteristic (Ohmic behavior) was observed (Figure 3a). The bare Au substrate shows the general metallic conductor (linear) property. However, pRNA-3WJ-SH (Figure 3b) exhibits the nonlinear *I*–*V* properties. Presumably, these biomolecules provide the energy band gap that makes the semiconducting behavior[39] and show the rectifying properties in the two-terminal system. Thus, it is hard to observe any resistive change effect in these molecules.

(1) Pt tip//pRNA-3WJ//Au substrate

When the QD/STV was adsorbed onto the Au surface, a slight resistive switching property was observed during the potential sweep (Figure 3c). It seems to form a double-tunnel junction configuration, such as the QD/STV/conducting Au substrate.

(2) Pt tip//QD/STV//Au substrate

Although a slight hysteresis is observed in the *I*–*V* curve of QD/STV, which depends on various factors such as the donor–acceptor pair or Schottky barrier effects, it mainly depends on the air gap between the tip and molecule.[40] The QD/STV/Au system shows a slight resistive switching property of the metal/molecule/metal tunneling junction, and the ON/OFF ratio was very weak and fluctuated. So it is difficult to use for resistive biomemory applications.

However, the QD/STV/Bio-3WJ-SH chimera shows a distinctive effect compared to QD/STV. The electrical bipolar switching behavior was observed. Presumably, the observed electrical bistability of the conjugated

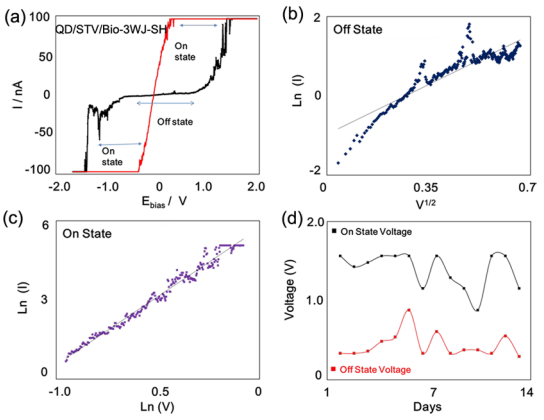

Figure 4. *I*–*V* characterization of the electrical bistability behavior. (a) *I*–*V* characteristics of the QD/STVQD/STV/Bio-3WJ-SH chimera on Au, exhibiting electrical bistability behavior where the current transition from low (OFF state) to high (ON state) and from low resistance to high resistance shows the memory effect. (b) Plot of ln(*I*)–$V^{1/2}$ fit for low conducting state, which was attributed to thermionic emission; (c) ln(*I*)–ln(*V*) fit for the high conductance state. The magnitudes of current and voltage have been plotted to show the reverse bias section of the characteristics. (d) Retention time and stability test of the QD/STV/Bio-3WJ-SH chimera on the Au substrate.

QD/STV/Bio-3WJ-SH chimera originated from the conjugation of pRNA-3WJ and QD/STV rather than an electronic phenomenon caused by either one of the two nanomaterials composing the chimera.

(3) Pt tip//QD/STV/Bio-3WJ-SH//Au substrate

Figure 3d shows the resistive switching effect of the QD/STV/Bio-3WJ-SH chimera, which can be observed when trace and retrace linear voltage scans are applied from 0 to −3.0 V and −3.0 to 0 V, respectively. Initially, the *I*–*V* curve of the chimera shows a low conductivity state, and this state was defined as "OFF". When the potential reaches 1.8 V, where an abrupt increase in conductivity occurs, this is defined as the "ON" state. This state indicates a transition of the chimera molecule from an initial OFF state to an ON state that is equivalent to the "writing" process in a digital resistive memory device. The high conductive state was retained over 1.8 V. Thus, the threshold voltage (V_{Th}) for switching is 1.8 V. When a negative voltage is applied continuously, the chimera molecule remains in the ON state until 0.3 V. Then, it returns to the low conductivity state (OFF state). This reverse voltage state is equivalent to the "erase" process in the memory device. Moreover, additional experiments were carried out to analyze the characteristics of current–distance characteristics (*I*–*s*) (Supporting Information Figure S2), and that of its derivatives is explained in the Supporting Information (Figure S3 and Table S1).

Resistive Biomemory Characteristics of the QD/STV/Bio-3WJ-SH Hybrid. To investigate the resistive switching mechanism based on trap and release of charge, biomemory function was analyzed. Figure 4a describes the *I*–*V* characteristics of QD/STV/Bio-3WJ-SH when a

bias voltage is applied from +3 to −3 V. As shown in the figure, the device starts switching to a conductive state (ON state) when the applied voltage is +1 V, with a sharp increase in the current, and remains in that state until the reverse voltage is applied. The device shows electrical hysteresis behavior that is an essential feature of bistable devices. State "1" and state "0" correspond to the relatively high current (ON state) and the relatively low current states (OFF state), respectively. The bistable transition from the OFF state to the ON state is equivalent to the "writing" process in a digital memory cell. After transition is achieved, the ON state remains in the device even after power is turned off. In presence of the QD/STV/Bio-3WJ-SH chimera system, the CdSe core in the QD and the pRNA-3WJ are separated by a large energy gap ZnS semiconductor tunneling barrier. The pRNA-3WJ behaves as the charge donor during the conductivity switching, allowing charge transfer to the lower-energy core.[40−43] We assume that an electric-field-induced charge transfer mechanism between the polyanionic pRNA-3WJ and the QD core is responsible for the observed electrical bistability of QD/STV/Bio-3WJ-SH chimeras. Figure 4 shows a study of the conduction mechanism in both the ON and OFF states of the RNA−QD chimera. To understand the conducting mechanism through the device, the *I*−*V* curves of this device in both states were analyzed in terms of theoretical models.

The plot of log(*I*) as a function of $V^{1/2}$ (Figure 4b) was fitted to a straight line, which suggests that the conduction mechanism is probably due to thermionic emission. Therefore, the conduction mechanism in the low conductivity state is dominated by charge injection from the electrode to the pRNA-3WJ. A linear curve was obtained between log(*I*) and $V^{1/2}$ (Figure 4b) from 0 to 0.7 V for the device in the OFF state. The *I*−*V* relationship in the OFF state of the QD/STV/Bio-3WJ-SH chimera could be explained with the injection-dominated thermionic emission model.[41] Accordingly, current density (J) at a particular filed F (=V/d) is given by

$$J = AT^2 \exp\left[\frac{\phi(e^3/4\pi\varepsilon)^{1/2}F^{1/2}}{KT}\right]$$

where *A* is a constant, ϕ is the barrier with the electrode, *e* is the electronic charge, ε is the permittivity of the active material, and *T* is the temperature. In Figure 4b, the plot of ln(*I*) *versus* $V^{1/2}$ was fitted to a linear model with mostly similar slopes, which aligns with the suggested model.[41] The *y*-axis intercept depends on the barrier height with the electrode. This suggests that the OFF current is controlled by charge injection from the Pt electrode, which is due the difference in the energy levels. Thus, an energy barrier between the Pt electrode and the QD/STV/Bio-3WJ-SH layer and the charge injection through the energy barrier dominate the conduction mechanism. It was varied with the active material in the biomemory device, for example, the streptavidin-coated ZnS shell thickness on CdSe or the pRNA-3WJ conjugated with the nanoparticles. This could be due to a decrease in the effective band gap of the core−shell nanoparticles that determines the barrier height with the electrode.

In the case of the ON state, the *I*−*V* relationship is changed for the pRNA-3WJ−QD chimera, which shows Ohmic behavior, a linear relation was also observed from the plot of log(*I*) as a function of log(*V*) in the high conductivity state, as shown in Figure 4c. From this plot, it can be observed that a space-charge-limited conduction (SCLC) emission is likely to be the conduction mechanism in the high conductivity state. The current flows through a pRNA-3WJ−QD chimera conduction path. The space-charge-limited current is given by the Mott-Gurne law[10]

$$J = \frac{8\varepsilon\mu v^2}{9d^3}$$

where μ is the carrier mobility and *d* is the thickness.

The higher bias voltage helps overcome the high band gap ZnS cap potential barrier by tunneling and injects electrons into the CdSe core. When a threshold voltage is reached (*i.e.*, 1.8 V), the applied potential enables tunneling into the CdSe core, causing a high conductance switch. Hysteresis was observed in return scanning from high to low bias, suggesting the presence of a small amount of charge storage in the QD core. Increase in potential induced strong SCLC because more injection carriers from the electrode results in more accumulated carriers at the interface between the electrode and RNA. Therefore, we can hypothesize that the current conduction changed from an injection-dominated mechanism in the low conductivity state to a charge-injection-dominated mechanism in the high conductivity state. It is assumed that the charge transfer process is the result of the charge-donating ability of the RNA, which enables the observed bistability behavior while it also provides a direct pathway to the charge transfer phenomenon. Therefore, a charge transport mechanism occurs during the transition between the conducting states. This proposed mechanism is similar to that of the devices using other materials, related to charge acceptor and donor behaviors of many bistable resistive memory devices.[44,45]

To confirm the stability of the pRNA-3WJ/QD chimera for use as a resistive biomemory device, the retention time test of pRNA-3WJ/QD chimera layer was conducted using STS. The *I*−*V* curve of the QD/STV/Bio-3WJ-SH chimera measurement was conducted at room temperature (Figure 4d). The potential sweep cycles were applied to determine the write and erase voltages for the device ON and OFF states, respectively. The retention time test was continued to 13 days in air, after which the

QD/STV/Bio-3WJ-SH chimera interface was becoming damaged and degraded through joule heating and contaminating the chimera molecule during the operation of the device.

CONCLUSION

In summary, we report the development of the pRNA-3WJ/QD chimera nanoparticle using an RNA aptamer-based method for the resistive biomolecular memory application. The pRNA-3WJ motif was redesigned to introduce both the Sephdaex G100-recognized aptamer and the biotin strand. The Sephadex G100 aptamer-based conjugation method provides a specific binding ratio between QD/STV and Bio-3WJ. This unique bioinorganic chimera nanoparticle exhibits electrical bistability at the nanoscale for the resistive biomolecular memory function, and this electrical property was well retained for 13 days. The present study shows that the use of the QD/STV/Bio-3WJ-SH chimera provides the possibility of biomolecular electronic apparatus application. The QD/STV/Bio-3WJ-SH chimera displayed potential for applications in next-generation nonvolatile nano-bioelectronic devices. In the near future, the RNA−inorganic chimera materials can be further developed into candidates for nano-bioelectronic devices such as information storage devices, logic gates, processing devices, and, eventually, nano-biocomputing systems.

MATERIALS AND METHODS

Materials. The grain-controlled ultraflat Au substrate (Platypus template-stripped gold chips) was purchased from Platypus Technologies (USA) for STM and STS. Mica was purchased from Ted Pella (USA) for atomic force microscopy. After immobilization, the substrate was washed with diethylpyrocarbonate (DEPC)-treated water (Sigma-Aldrich, USA) and then dried with N_2 gas. The QD/STV (CdSe−ZnS, 655 nm) nanoparticles were purchased from Life Technology (USA). The Sephadex G100 resin was purchased from Sigma-Aldrich (USA). The binding buffer (50 mM HEPES, 150 mM NaCl, 10 mM $MgCl_2 \cdot 6H_2O$) and the elution buffer (4 M urea, 5 mM EDTA) were prepared for conjugation. Milli-Q water (DDW >18 MΩ) was used for all experiments.

***In Vitro* Synthesis and Purification of pRNA-3WJ.** The pRNA-3WJ-a and 5′-end biotin-labeled pRNA-3WJ-b (Bio-3WJ-b), DNA 3WJ-b, and 5′-end thiol-labeled pRNA-3WJ-c (SH-3WJ-c) were chemically synthesized by Integrated DNA Technologies (USA) (see Supporting Information Table S1). A Sephadex G100 binding RNA aptamer sequence was added to the 3′-end of pRNA-3WJ-c (Figure 2a).[35] The Sephadex G100 RNA aptamer 3WJ-c (SEPapt-3WJ-c) was then synthesized by *in vitro* transcription of the corresponding DNA template by T7 RNA polymerase.[12,36]

Construction of the pRNA-3WJ Nanoparticle with Sephadex Aptamer and Biotin. The pRNA-3WJ nanoparticle with the Sephadex aptamer and biotin (SEPapt/Bio-3WJ) was assembled by annealing three corresponding RNA strands at equal molar ratio in TMS buffer (40 mM Tris-HCl, 10 mM $MgCl_2$, 100 mM NaCl) by heating at 80 °C for 5 min, followed by slowly cooling to 4 °C at a rate of 2 °C/min on a Master cycle thermocycler (Eppendorf, Germany). The nanoparticle assembly was confirmed by 8% native polyacrylamide gel prepared in TBM buffer (89 mM Tris, 200 mM boric acid, 5 mM $MgCl_2$, pH 7.6). About 0.2 μg of RNA samples was loaded into each lane. After being run at 80 V at 4 °C for 2 h, the RNA nanoparticles were visualized by fluorescence signal or ethidium bromide staining, with images captured by Typhoon FLA 7000 (GE Healthcare, UK).

RNA Aptamer-Based Conjugation between QD/STV and Bio-3WJ. The RNA aptamer-based conjugation technique was carried out for the production of the pRNA-3WJ/QD chimera (Figure 1a). The first step is to immobilize the SEPapt/Bio-3WJ complex onto the Sephadex G100 resin through the aptamer recognition reaction. Simply, the SEPapt/Bio-3WJ complex (1 μM) was mixed with the Sephadex G100 resin (50 mg) in binding buffer and incubated for 12 h at 4 °C with shaking. The SEPapt/Bio-3WJ complex immobilized to the G100 resins was then washed three times by centrifugation with binding buffer. Then, 300 μL of 400 nM streptavidin-coated QD (QD/STV, CdSe/ZnS, 655 nm) was added with gentle shaking at 4 °C in the dark for 6 h. The QD/STV was bound to the SEPapt/Bio-3WJ complex that was immobilized on G100 resins through streptavidin and biotin interaction. Unreacted QD/STV was washed out by centrifugation with binding buffer three times. Finally, the QD/STV/Bio-3WJ-b was released from G100 resins by adding elution buffer containing 4 M urea and 5 mM EDTA with gentle mixing for approximately 30 min; this step was repeated five times to increase the recovery yield. Then, the QD/STV/Bio-3WJ-b fragment and SEPapt/3WJ-c and DNA 3WJ-a fragments were dissociated in elution buffer to separate the QD/STV/Bio-3WJ-b and other 3WJ fragments from G100 resins. The eluent containing QD/STV/Bio-3WJ-b was purified using an Amicon Ultra centrifugal filter (MWCO 10K, Millipore, USA). QD/STV/Bio-3WJ-b was reassembled into QD/STV/Bio-3WJ-SH by incubating with 3WJ-a and SH-3WJ-c to acquire a final 3WJ/QD nanoparticle with all three 3WJ-a-b-c fragments for further experiments.

Surface Characterization for Confirmation of QD/STV/Bio-3WJ-SH Chimera Nanoparticles. To test the electrical property of the SH-modified QD/STV/Bio-3WJ-SH chimera at the nanoscale, the chimera samples were diluted to 2 nM in TMS buffer (50 mM Tris, 100 mM NaCl, 10 mM $MgCl_2$). The droplet of samples (10 μL) was immediately self-assembled on an ultraflat Au substrate through covalent bonding between the SH group and Au. After a 10 min incubation period on the specifically modified Au surface,[36] excess samples were washed with DEPC-treated water and dried under a flow of N_2 gas. STM and STS measurements were performed on a Digital Instruments Multimode STM using a Nanoscope III controller (Veeco, CA, USA). Measurements were conducted under ambient conditions using mechanically cut Pt tips.

Electrical Measurements of QD/STV/Bio-3WJ-SH Chimera Nanoparticles. For *I*−*V* measurements, the STM tip was located above the spot to be measured. No additional force was applied to the tip, and the same set point of 0.5 nA with a bias voltage of 0.1 V was used for all experiments. All the electrical measurements on the single QD/STV/Bio-3WJ-SH chimera were performed by STM under an open air environment at ambient conditions. The tunneling current was observed as the tip−sample bias was ramped in the range of ±3 V. The shape of the *I*−*V* curve depends on the STM tip position over the QD/STV/Bio-3WJ-SH chimera where the current is measured. In a typical electrical characterization experiment, a "point and shoot" method was used to directly place the STM tip (Pt/Ir) on a single QD/STV/Bio-3WJ-SH chimera. All measurements were carried out by first taking a morphology scan of an individual molecule of the assembled QD/STV/Bio-3WJ-SH chimera. Then the STM tip was positioned on the top of a single QD/STV/Bio-3WJ-SH chimera. For the purpose of the electrical characterization at the nanoscale, the ultraflat Au substrate (Platypus template-stripped gold chips) was used as the bottom electrode while the 14 mm length of the conductive STM tip was used as the top electrode for the two-terminal system.

Conflict of Interest: The authors declare the following competing financial interest(s): Peixuan Guo is a co-founder of Biomotor and RNA Nanotechnology Development Corp. Ltd.

Acknowledgment. The authors thank M. Vieweger for comments on the project. This research was supported by Leading Foreign Research Institute Recruitment Program through the National Research Foundation of Korea (NRF) funded by the Ministry of Science, ICT & Future Planning (MSIP) (2013K1A4A3055268), and NIH grants U01CA151648 and R01EB012135 to P.G. Funding to P.G.'s Endowed Chair in Nanobiotechnology position is by the William Fairish Endowment Fund. P.G. is a co-founder of Biomotor and RNA Nanotechnology Development Corp. Ltd.

Supporting Information Available: Surface investigation of pRNA-3WJ, QD/STV, QD/STV/Bio-3WJ-SH conjugate by STM, and current−distance characteristics of the QD/STV/Bio-3WJ-SH hybrid nanoparticles. The Supporting Information is available free of charge on the ACS Publications website at DOI: 10.1021/acsnano.5b03269.

REFERENCES AND NOTES

1. Moore, G. E. Cramming More Components Onto Integrated Circuits (Reprinted from Electronics, pp 114−117, April 19, 1965). *Proc. IEEE* **1998**, *86*, 82−85.
2. Petty, M. C. Scope of Molecular Electronics. In *Molecular Electronics: From Principles to Practice*, 1st ed.; Petty, M. C., Ed.; Wiley: West Sussex, U.K., 2008.
3. Kim, T. W.; Lee, K.; Oh, S. H.; Wang, G.; Kim, D. Y.; Jung, G. Y.; Lee, T. A Direct Metal Transfer Method for Cross-Bar Type Polymer Non-Volatile Memory Applications. *Nanotechnology* **2008**, *19*, 405201.
4. Heath, J. R. Molecular Electronics. *Annu. Rev. Mater. Res.* **2009**, *39*, 1–23.
5. Lu, W.; Lieber, C. M. Nanoelectronics From the Bottom Up. *Nat. Mater.* **2007**, *6*, 841–850.
6. Tseng, R. J.; Tsai, C. L.; Ma, L. P.; Ouyang, J. Y. Digital Memory Device Based on Tobacco Mosaic Virus Conjugated With Nanoparticles. *Nat. Nanotechnol.* **2006**, *1*, 72–77.
7. Offenhausser, A.; Rinaldi, R. *Nanobioelectronics—For Electronics, Biology, and Medicine*; Springer: New York, 2009.
8. Noy, A. Bionanoelectronics. *Adv. Mater. (Weinheim, Ger.)* **2011**, *23*, 807–820.
9. Cho, B.; Song, S.; Ji, Y.; Kim, T. W.; Lee, T. Organic Resistive Memory Devices: Performance Enhancement, Integration, and Advanced Architectures. *Adv. Funct. Mater.* **2011**, *21*, 2806–2829.
10. Ko, Y.; Kim, Y.; Baek, H.; Cho, J. Electrically Bistable Properties of Layer-by-Layer Assembled Multilayers Based on Protein Nanoparticles. *ACS Nano* **2011**, *5*, 9918–9926.
11. Strukov, D. B.; Kohlstedt, H. Resistive Switching Phenomena in Thin Films: Materials, Devices, and Applications. *MRS Bull.* **2012**, *37*, 108–117.
12. Guo, P. The Emerging Field of RNA Nanotechnology. *Nat. Nanotechnol.* **2010**, *5*, 833–842.
13. Shu, D.; Shu, Y.; Haque, F.; Abdelmawla, S.; Guo, P. Thermodynamically Stable RNA Three-Way Junctions for Constructing Multifuntional Nanoparticles for Delivery of Therapeutics. *Nat. Nanotechnol.* **2011**, *6*, 658–667.
14. Guo, P.; Zhang, C.; Chen, C.; Trottier, M.; Garver, K. Inter-RNA Interaction of Phage Phi29 PRNA to Form a Hexameric Complex for Viral DNA Transportation. *Mol. Cell* **1998**, *2*, 149–155.
15. Guo, P.; Erickson, S.; Anderson, D. A Small Viral RNA Is Required for *in Vitro* Packaging of Bacteriophage Phi29 DNA. *Science* **1987**, *236*, 690–694.
16. Shu, Y.; Haque, F.; Shu, D.; Li, W.; Zhu, Z.; Kotb, M.; Lyubchenko, Y.; Guo, P. Fabrication of 14 Different RNA Nanoparticles for Specific Tumor Targeting Without Accumulation in Normal Organs. *RNA* **2013**, *19*, 767–777.
17. Shu, D.; Moll, W. D.; Deng, Z.; Mao, C.; Guo, P. Bottom-Up Assembly of RNA Arrays and Superstructures As Potential Parts in Nanotechnology. *Nano Lett.* **2004**, *4*, 1717–1723.
18. Shu, Y.; Shu, D.; Haque, F.; Guo, P. Fabrication of PRNA Nanoparticles to Deliver Therapeutic RNAs and Bioactive Compounds into Tumor Cells. *Nat. Protoc.* **2013**, *8*, 1635–1659.
19. Binzel, D. W.; Khisamutdinov, E. F.; Guo, P. Entropy-Driven One-Step Formation of Phi29 PRNA 3WJ From Three RNA Fragments. *Biochemistry* **2014**, *53*, 2221–2231.
20. Haque, F.; Shu, D.; Shu, Y.; Shlyakhtenko, L.; Rychahou, P.; Evers, M.; Guo, P. Ultrastable Synergistic Tetravalent RNA Nanoparticles for Targeting to Cancers. *Nano Today* **2012**, *7*, 245–257.
21. Liu, J.; Guo, S.; Cinier, M.; Shlyakhtenko, L. S.; Shu, Y.; Chen, C.; Shen, G.; Guo, P. Fabrication of Stable and RNase-Resistant RNA Nanoparticles Active in Gearing the Nanomotors for Viral DNA Packaging. *ACS Nano* **2011**, *5*, 237–246.
22. Khisamutdinov, E. F.; Jasinski, D. L.; Guo, P. RNA As a Boiling-Resistant Anionic Polymer Material to Build Robust Structures With Defined Shape and Stoichiometry. *ACS Nano* **2014**, *8*, 4771–4781.
23. Khisamutdinov, E.; Li, H.; Jasinski, D.; Chen, J.; Fu, J.; Guo, P. Enhancing Immunomodulation on Innate Immunity by Shape Transition Among RNA Triangle, Square, and Pentagon Nanovehicles. *Nucleic Acids Res.* **2014**, *42*, 9996–10004.
24. Chworos, A.; Severcan, I.; Koyfman, A. Y.; Weinkam, P.; Oroudjev, E.; Hansma, H. G.; Jaeger, L. Building Programmable Jigsaw Puzzles With RNA. *Science* **2004**, *306*, 2068–2072.
25. Afonin, K. A.; Viard, M.; Koyfman, A. Y.; Martins, A. N.; Kasprzak, W. K.; Panigaj, M.; Desai, R.; Santhanam, A.; Grabow, W. W.; Jaeger, L.; Heldman, E.; Reiser, J.; Chiu, W.; Freed, E. O.; Shapiro, B. A. Multifunctional RNA Nanoparticles. *Nano Lett.* **2014**, *14*, 5662–5671.
26. Lee, J. B.; Hong, J.; Bonner, D. K.; Poon, Z.; Hammond, P. T. Self-Assembled RNA Interference Microsponges for Efficient SiRNA Delivery. *Nat. Mater.* **2012**, *11*, 316–322.
27. Stephenson, W.; Asare-Okai, P. N.; Chen, A. A.; Keller, S.; Santiago, R.; Tenenbaum, S. A.; Garcia, A. E.; Fabris, D.; Li, P. T. The Essential Role of Stacking Adenines in a Two-Base-Pair RNA Kissing Complex. *J. Am. Chem. Soc.* **2013**, *135*, 5602–5611.
28. Leontis, N. B.; Westhof, E. Chemistry. Self-Assembled RNA Nanostructures. *Science* **2014**, *345*, 732–733.
29. Hsu, B. B.; Hagerman, S. R.; Jamieson, K.; Veselinovic, J.; O'Neill, N.; Holler, E.; Ljubimova, J. Y.; Hammond, P. T. Multilayer Films Assembled From Naturally-Derived Materials for Controlled Protein Release. *Biomacromolecules* **2014**, *15*, 2049–2057.
30. Sun, H.; Sheng, J.; Hassan, A. E.; Jiang, S.; Gan, J.; Huang, Z. Novel RNA Base Pair With Higher Specificity Using Single Selenium Atom. *Nucleic Acids Res.* **2012**, *40*, 5171–5179.
31. Shopsowitz, K. E.; Roh, Y. H.; Deng, Z. J.; Morton, S. W.; Hammond, P. T. RNAi-Microsponges Form Through Self-Assembly of the Organic and Inorganic Products of Transcription. *Small* **2014**, *10*, 1623–1633.
32. Westhof, E. Isostericity and Tautomerism of Base Pairs in Nucleic Acids. *FEBS Lett.* **2014**, *588*, 2464–2469.
33. Moll, D.; Guo, P. Grouping of Ferritin and Gold Nanoparticles Conjugated to PRNA of the Phage Phi29 DNA-Packaging Motor. *J. Nanosci. Nanotechnol.* **2007**, *7*, 3257–3267.
34. Jung, D.; Minami, I.; Patel, S.; Lee, J.; Jiang, B.; Yuan, Q.; Li, L.; Kobayashi, S.; Chen, Y.; Lee, K. B.; Nakatsuji, N. Incorporation of Functionalized Gold Nanoparticles into Nanofibers for Enhanced Attachment and Differentiation of Mammalian Cells. *J. Nanobiotechnol.* **2012**, *10*, 23.
35. Srisawat, C.; Goldstein, I.; Engelke, D. Sephadex-Binding RNA Ligands: Rapid Affinity Purification of RNA From Complex RNA Mixtures. *Nucleic Acids Res.* **2001**, *29*, 4e.
36. Jasinski, D.; Khisamutdinov, E. F.; Lyubchenko, Y. L.; Guo, P. Physicochemically Tunable Poly-Functionalized RNA Square Architecture With Fluorogenic and Ribozymatic Properties. *ACS Nano* **2014**, *8*, 7620–7629.
37. Ponchon, L.; Dardel, F. Recombinant RNA Technology: the TRNA Scaffold. *Nat. Methods* **2007**, *4* (7), 571–576.
38. Ponchon, L.; Dardel, F. Large Scale Expression and Purification of Recombinant RNA in Escherichia Coli. *Methods* **2011**, *54*, 267–273.

39. Smith, A. M.; Nie, S. Semiconductor Nanocrystals: Structure, Properties, and Band Gap Engineering. *Acc. Chem. Res.* **2010**, *43*, 190–200.
40. Jortner, J.; Bixon, M.; Langenbacher, T.; Michel-Beyerle, M. E. Charge Transfer and Transport in DNA. *Proc. Natl. Acad. Sci. U. S. A.* **1998**, *95*, 12759–12765.
41. Chu, C. W.; Ouyang, J.; Tseng, H. H.; Yang, Y. Organic Donor-Acceptor System Exhibiting Electrical Bistability for Use in Memory Devices. *Adv. Mater. (Weinheim, Ger.)* **2005**, *17*, 1440–1443.
42. Voityuk, A. A. Electronic Coupling for Charge Transfer in Donor-Bridge-Acceptor Systems. Performance of the Two-State FCD Model. *Phys. Chem. Chem. Phys.* **2012**, *14*, 13789–13793.
43. Zhang, Y.; Zherebetskyy, D.; Bronstein, N. D.; Barja, S.; Lichtenstein, L.; Schuppisser, D.; Wang, L. W.; Alivisatos, A. P.; Salmeron, M. Charge Percolation Pathways Guided by Defects in Quantum Dot Solids. *Nano Lett.* **2015**, *15*, 3249.
44. Kim, T. W.; Yang, Y.; Li, F. S.; Kwan, W. L. Electrical Memory Devices Based on Inorganic/Organic Nanocomposites. *NPG Asia Mater.* **2012**, *4*, e18.
45. Ribierre, J. C.; Aoyama, T.; Muto, T.; Andre, P. Hybrid Organic-Inorganic Liquid Bistable Memory Devices. *Org. Electron.* **2011**, *12*, 1800–1805.